Journal of Magnetism and Magnetic Materials 86 (1990) 349–362
North-Holland

MAGNETIC STRUCTURES OF $RMnSi_2$ COMPOUNDS (R = La, Ce, Pr, Nd) FROM NEUTRON STUDY

B. MALAMAN, G. VENTURINI

Laboratoire de Chimie du Solide Mineral, Université de Nancy I, Associé au CNRS UA 158, BP 239, 54506 Vandoeuvre-les-Nancy Cedex, France

L. PONTONNIER and D. FRUCHART

Laboratoire de Cristallographie du CNRS, Associé à l'Université J. Fourier, 166X, 38042 Grenoble Cedex, France

Received 3 August 1989

Investigations by neutron diffraction measurements are reported on the ternary silicides $RMnSi_2$ (R = La to Nd) with the orthorhombic structure of $TbFeSi_2$ type (SG:Cmcm). This structure, closely related to the $ThCr_2Si_2$ type structure, can be described as isolated $ThCr_2Si_2$ blocks connected via α $ThSi_2$ slabs. Each of the R, Mn and Si atoms are arranged in alternate layers stacked (along the *b*-axis) with the sequence $RSi(Mn_2)SiRSiSiRSi(Mn_2)SiR$. The Mn–Mn intralayer distances (~ 2.9Å) are considerably shorter than the Mn–Mn interlayers distances (~ 9Å). At room temperature, all four compounds order ferromagnetically. The magnetic moments of Mn atoms ($\sim 2\mu_B$) are parallel to the *b*-axis. At lower temperatures $PrMnSi_2$ and $NdMnSi_2$ show an additional magnetic transition which corresponds to the ordering of the rare-earth sublattice. $PrMnSi_2$ orders antiferromagnetically below $T_N = 35$ K; its magnetic structure consists of ferromagnetic (010) layers of Pr and Mn with moments perpendicular to the layers. Each Mn layer is antiferromagnetically coupled to the two adjacent ferromagnetically coupled Pr layers ($\mu_{Mn} = 2.35(10)\mu_B$, $\mu_{Pr} = 2.04(4)\mu_B$). Below $T_C = 40$ K, $NdMnSi_2$ is still ferromagnetic. Nd and Mn magnetic moments lie in the (011) plane, along [001] and at 45° of this direction for Nd and Mn, respectively ($\mu_{Mn} = 2.25(10)\mu_B$, $\mu_{Nd} = 1.80(7)\mu_B$). At 2 K, a preliminary study shows that, in $CeMnSi_2$, the cerium sublattice would be ferromagnetic and antiferromagnetically coupled with the manganese sublattice according to the following scheme: $-(+)-\,-(+)-$, reference to the stacking sequence previously defined ($\mu_{Mn} = 2.24(15)\mu_B$, $\mu_{Ce} = 0.23(13)\mu_B$). The results are discussed in terms of RKKY exchange interactions and compared with those obtained previously on the corresponding $ThCr_2Si_2$ type ternary silicides and germanides.

1. Introduction

The $RMnSi_2$ silicides (R = La to Sm) crystallize in the $TbFeSi_2$ type structure [1]. This structure is orthorhombic (space group Cmcm) and can be described as built of alternating (010) planes containing R, Mn and Si atoms, respectively, in a R Si Mn Si R Si Si R Si Mn Si ··· sequence. This structure is therefore closely related to the $ThCr_2Si_2$-type structure [2] (space group I4/mmm) in which the same atoms lie in alternate layers stacked along *c*-axis with the sequence Th Si Cr Si Th Si Cr Si Th ···. Fig. 1 shows the blocks which are common to the two structures. In both cases, the Si atoms form tetrahedra around the transition metal atoms T, and the T–Si distances are very short, suggesting covalent bonding. In other words, theses structures exhibit structural relationships with the α $ThSi_2$ type structure [3] by insertion of transition metal planes. α $ThSi_2$ may be described as $ThSi_8$ tetragonal prisms sharing edges and faces in the (001) planes and stacked along [001] with the following sequence ··· Si Th Si ···. A shift (*a*/2 or *b*/2) between each adjacent (001) plane yields the formation of Si_4 tetrahedral sites which are filled by the T atoms. Thus, we obtain the $ThCr_2Si_2$ type structure. When this operation occurs only for half of the planes, we get the $TbFeSi_2$ type structure which then may be considered as a stacking of both $ThCr_2Si_2$ and α $ThSi_2$ slabs. Fig.

0304-8853/90/$03.50 © 1990 – Elsevier Science Publishers B.V. (North-Holland)

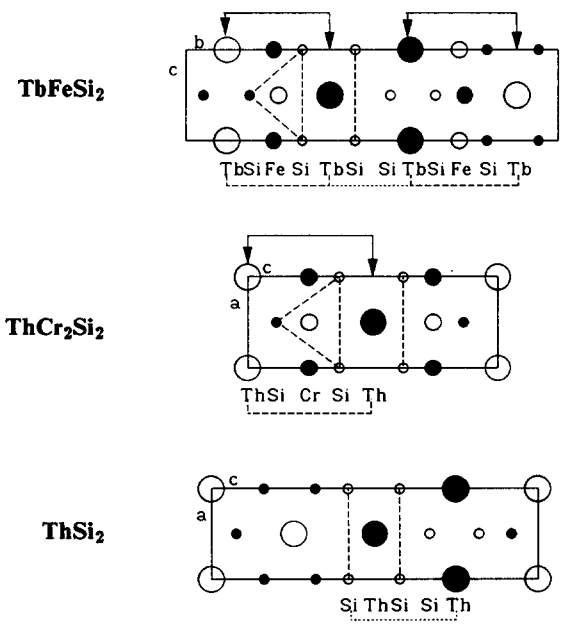

Fig. 1. Structures of $TbFeSi_2$, $ThCr_2Si_2$ and α $ThSi_2$. Structural relationships.

1 shows these structural relationships.

In both $ThCr_2Si_2$ and $TbFeSi_2$ type structures, the R and T atoms form a square (or nearly) network with R–R and T–T distances close to 4 and 2.9 Å, respectively. The T–T interlayer distances are larger. They are of about 5.4 Å in the RMn_2X_2 compounds and considerably larger (~ 9Å) in the $RMnSi_2$ compounds. Therefore, the $TbFeSi_2$ structure can be seen as a still more anisotropic variant of the $ThCr_2Si_2$ structure.

During the past ten years, the magnetic properties of RMn_2Si_2 and RMn_2Ge_2 compounds have been extensively studied by magnetometric and neutron diffraction techniques (see ref. [4] where a large review on the physical properties of these compounds can be found). They deserve special attention, since their main characteristic is the presence of long-range ordering of the manganese moments. The magnetic ordering of the manganese sublattice persists up to temperatures higher than 300 K, while the rare earth sublattice shows eventually magnetic ordering at low temperature only [4]. Since T = Mn is the unique example of a 3d transition metal sharing a magnetic moment, the RMn_2X_2 (X = Si, Ge) series have been the subject of more careful investigations in order to determine the respective magnitudes of the Mn–R, Mn–Mn and R–R couplings [4].

Table 1
$RMnSi_2$ compounds. Magnetic data [5] and observed magnetic moments, with 150 kOe, versus temperature. Values extrapolated to infinite field, at 4.2 K (within brackets)

Compounds	Transition temperatures (K)		Θ_p	μ_{eff} ($\mu_B mol^{-1}$)	$\mu_{theo} R^{3+}$ (μ_B)		$\mu_{eff} R^{3+}$ (μ_B) [b]
	T_C	T_N			Hund	Van Vleck	
$LaMnSi_2$	386		395	2.6	0	0	
$CeMnSi_2$	398		420	3.52	2.54	2.56	2.39
$PrMnSi_2$	434	35	450	4.29	3.58	3.62	3.42
$NdMnSi_2$	40–441		460	4.41	3.62	3.68	3.57
$SmMnSi_2$	464		482	3.02	0.84	1.60	1.55

Compounds	$\mu = f(1/H)$ at			gJ (R^{3+} ion)
	4.2 K	200 K	300 K	
$LaMnSi_2$	1.61 (1.80)	1.51	1.32	0
$CeMnSi_2$	1.72 (2.00)	1.60	1.42	2.14
$PrMnSi_2$	3.75 [b] (4.00)	1.82	1.59	3.20
$NdMnSi_2$	3.68 (4.10)	1.97	1.70	3.27
$SmMnSi_2$	1.74 (1.90)	1.46	1.34	0.71

[a] $\mu_{eff} Mn = 2.6\mu_B$.
[b] Metamagnetic transition at 28 kOe.

From this point of view, it was rather interesting to study the magnetic properties of the $RMnSi_2$ compounds at the light of their more anisotropic layered structure.

Magnetic measurements on $RMnSi_2$ (R = La to Sm) polycrystalline samples have been largely described [5]. In the whole series, the manganese sublattice orders ferromagnetically up to rather high temperatures: T_C increases from 386 to 464 K between $LaMnSi_2$ and $SmMnSi_2$. At lower temperatures, $PrMnSi_2$ and $NdMnSi_2$ show an additional magnetic transition which corresponds to the ordering of the rare-earth sublattices. $PrMnSi_2$ becomes antiferromagnetic below T_N = 35 K while $NdMnSi_2$ remains ferromagnetic (T_C' = 40 K). The main characteristic magnetic data are collected in table 1.

In this paper, we report on the magnetic structures of $LaMnSi_2$, $CeMnSi_2$, $PrMnSi_2$ and $NdMnSi_2$ from neutron diffraction experiments. A comparison with the isotype $RFeSi_2$ and RMn_2X_2 (R = La to Sm; X = Si, Ge) compounds and a more general discussion are given in the conclusion.

2. Sample preparation

All the compounds were prepared from commercially available high-purity elements: Mn (powder, 99.9%), rare earth (R) elements (ingots, 99.9%) and silicon (powder, 99.99%). Pellets of starting composition $RMnSi_2$ (R = La, Ce, Pr or Nd) were compacted using a steel die, and were annealed several times (with grinding and compacting each time) at 1273 K in sealed silica tubes under argon (0.2 atm) and finally quenched in water. Purity of the final samples was determined by X-ray diffraction technique using a Guinier camera (Cu Kα).

3. Structure determination

The X-ray diffraction patterns obtained from powder samples show that all these compounds are single phase materials, with the $TbFeSi_2$ type structure. The R, Mn and Si atoms occupy 4(c) sites of mm point symmetry. In a previous paper, refinement of the $LaMnSi_2$ structure by using powder X-ray experiments has been reported [5]. We have clearly confirmed that our samples belong to the $TbFeSi_2$ type structure and that a possible mixing between Mn and Si atoms is totally excluded. In the following, the nuclear intensities will be calculated using, as a starting point, the atomic positions refined in the case of $LaMnSi_2$. The atomic positions of $LaMnSi_2$ and the lattice parameters of all the samples are given in table 2.

Table 2
$RMnSi_2$ compounds

Compounds	a (Å)	b (Å)	c (Å)	V (Å^3)
$LaMnSi_2$	4.191 (3)	17.68 (1)	4.073 (3)	302
$CeMnSi_2$	4.123 (3)	17.55 (1)	4.035 (3)	292
$PrMnSi_2$	4.094 (3)	17.55 (1)	4.028 (3)	289
$NdMnSi_2$	4.072 (3)	17.49 (1)	4.017 (3)	286
$SmMnSi_2$	4.035 (3)	17.41 (1)	3.998 (3)	281

$LaMnSi_2$ compound atomic positions (space group: Cmcm)

Atom	Site	Symmetry	x	y	z
La	4 (c)	mm	0	0.1052 (6)	$\frac{1}{4}$
Mn	4 (c)	mm	0	0.7478 (8)	$\frac{1}{4}$
Si_1	4 (c)	mm	0	0.455 (2)	$\frac{1}{4}$
Si_2	4 (c)	mm	0	0.316 (2)	$\frac{1}{4}$

4. Neutron diffraction

Neutron diffraction experiments were carried out at Institute Laue Langevin (ILL), Grenoble. The diffraction patterns were recorded with the one-dimension curved multidetector Dlb at a wavelength $\lambda = 2.5232$ Å. In each case, several patterns were collected in the temperature range 2–300 K (namely above and below the rare earth ordering temperature for $PrMnSi_2$ and $NdMnSi_2$). No pattern was collected in the paramagnetic state ($T_C > 400$ K). Using the Fermi lengths of ref. [6] and the magnetic form factors of Mn and R^{3+} ions of ref. [7], the scaling factor, the atomic positions y and the magnetic moments of Mn and R^{3+} were refined by using a least squares procedure [8]. The MXD program allows to simulta-

neously fit the nuclear and magnetic intensities to the observed quantities.

In each case, attempts were made to fit the nuclear contributions to the observed intensities by interchanging the position of the Mn and Si atoms, always leading to a poorer agreement and then confirming the crystallographic positions given by our previous X-ray powder diffraction studies [5].

Moreover, it is important to stress that the Mn sublattice is nearly a F lattice mode (table 2). Thus, the magnetic contributions to the observed intensities, due to a ferromagnetic ordering of the Mn atoms, practically affect the only nuclear lines obeying the extinction rule: (hkl) with h, k, l, of the same parity. In this case, it also becomes possible to check the crystal structure from refinement using the remaining lines only.

4.1. $LaMnSi_2$

Neutron diffraction patterns obtained at 300, 200 and 2 K (fig. 2) show only an increase in the intensities of the nuclear reflections which obey the rule: (h, k, l) with h, k, l of the same parity, which indicates the occurrence of ferromagnetic ordering of the Mn-sublattice.

Furthermore, the absence of magnetic contributions to the ($0k0$) reflections indicates that the moments are aligned along the b-axis. The values of the magnetic moments and of the y atomic positions obtained at 300, 200 and 2 K are presented in table 3 as well as the observed and calculated intensities. The thermal dependence of the neutron scattering, as deduced from patterns recorded step-by-step between 300 and 2 K, reveals a continuous variation of the magnetic moment in agreement with magnetometric measurements (table 1, [5]). The magnetic structure is shown in fig. 3. It corresponds to a stacking of ferromagnetic ($0k0$) sheets, with moments perpendicular to the sheets, ferromagnetically coupled along the (stacking) b-axis.

4.2. $CeMnSi_2$

Two neutron diffraction patterns have been recorded at 18 and 2 K. The results of neutron diffraction for this compound are similar to those for $LaMnSi_2$ (table 4), yielding the same ferromagnetic ordering onto the Mn-sublattice.

However, in agreement with the trivalent state of Ce-atom in this compound [5] (cf. section 1), magnetic ordering of the Ce-sublattice was to be

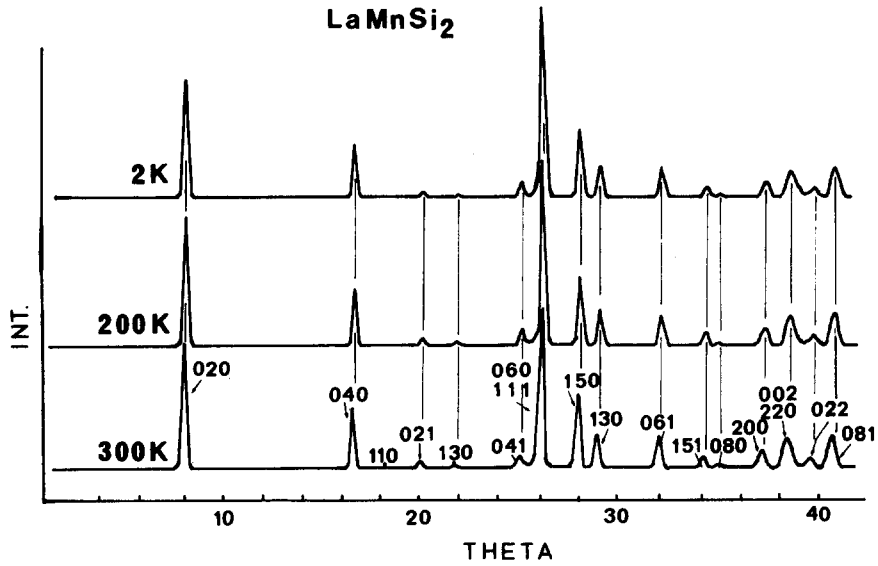

Fig. 2. Neutron diffraction patterns of $LaMnSi_2$ at 300, 200 and 2 K.

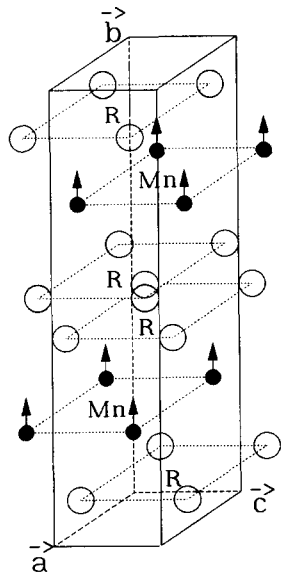

Fig. 3. Magnetic structure of $LaMnSi_2$. [*Magnetic structure of $RMnSi_2$ (R = Ce, Pr, Nd) compounds at high temperature.*]

considered, at least at 2 K. The results of the refinements, carried out in this direction, are collected in table 4. They display the presence of a very weak moment on cerium ($\mu_{Ce} = 0.23(12)\mu_B$). Moreover, the cerium sublattice would thus be ferromagnetic, and antiferromagnetically coupled with the manganese sublattice according to the following scheme: $-(+)-\ -(+)-$ [refer to the stacking sequence previously defined as Ce-(Mn)-Ce-Ce-(Mn)-Ce... (fig. 1)].

The very weak value of the moment might be due either to a too high temperature or to spin-fluctuation effects. A neutron diffraction pattern at a lower temperature, 1 K or less, should lift this ambiguous situation. This study is in progress.

4.3. $PrMnSi_2$

Three neutron diffraction patterns recorded at 300, 200 and 2 K are shown in fig. 4. At 300 and 200 K, i.e. above the ordering temperature of the

Table 3
$LaMnSi_2$. Calculated and observed intensities, y atomic positions, magnetic moments and reliability factors at 300, 200 and 2 K

hkl	300 K		200 K		2 K	
	y_{La} = 0.1018(5)	y_{Si1} = 0.3248(9)	y_{La} = 0.1011(5)	y_{Si1} = 0.3234(10)	y_{La} = 0.1016(6)	y_{Si1} = 0.3234(9)
	y_{Mn} = 0.7510(9)	y_{Si2} = 0.4651(12)	y_{Mn} = 0.7508(11)	y_{Si2} = 0.4649(14)	y_{Mn} = 0.7513(9)	y_{Si2} = 0.4642(10)
	I_0	I_c	I_0	I_c	I_0	I_c
020	34.29	34.00	34.27	34.25	34.20	34.10
040	52.37	52.47	50.44	50.70	52.13	52.51
110	~ 0.00	0.53	~ 0.00	0.64	~ 0.00	0.61
021	9.21	9.86	9.84	9.98	9.34	10.13
130	3.95	4.58	3.95	4.29	3.45	4.37
041	32.93	33.27	33.40	35.56	31.34	33.79
060 / 111	468.35	464.88	478.61	478.15	489.28	487.59
150	214.18	213.35	214.86	218.08	214.71	219.55
131	104.52	107.15	107.75	113.38	114.16	116.50
061	135.62	133.61	140.89	137.56	141.15	140.77
151	49.30	52.78	62.07	64.02	62.07	63.56
080	11.54	12.92	14.18	15.77	15.17	15.58
200	97.17	104.44	100.56	106.89	101.39	108.37
220 / 002	185.12	179.34	185.12	185.02	185.12	186.79
022	74.95	74.82	82.00	78.02	80.90	78.31
081	249.55	246.90	254.12	241.95	254.50	244.52
μ_{Mn} (μ_B)	1.77(19) //b		2.03(19) //b		2.07(19) //b	
R_w	1.9%		1.4%		2.1%	

Table 4
$CeMnSi_2$. Calculated and observed intensities, y atomic positions, magnetic moments and reliability factors at 18 and 2 K

hkl	18 K		2 K		2 K [a]	
	y_{Ce} = 0.1027(9)	y_{Si1} = 0.3231(10)	y_{Ce} = 0.1022(9)	y_{Si1} = 0.3237(10)	y_{Ce} = 0.1021(9)	y_{Si1} = 0.3243(9)
	y_{Mn} = 0.7527(16)	y_{Si2} = 0.4644(14)	y_{Mn} = 0.7518(13)	y_{Si2} = 0.4634(15)	y_{Mn} = 0.7512(12)	y_{Si2} = 0.4642(14)
	I_0	I_c	I_0	I_c	I_0	I_c
020	1299	1304	1563	1573	1563	1567
040	1309	1313	1575	1620	1575	1582
110	335	285	400	333	400	341
021	0	8	0	15	0	40
130	0	36	0	37	0	42
041	786	626	902	774	902	805
060	872	782	1017	870	1017	911
111	19282	19102	23025	22593	23025	22912
150	6262	6599	7241	7468	7241	7311
131	2468	2655	2779	3108	2779	2822
061	4460	4649	5250	5550	5250	5373
151	3453	3438	4167	4129	4167	4079
080	1344	1192	1532	1552	1532	1420
200	3822	3245	4551	3838	4551	3696
220 / 002	6318	6468	7445	7657	7445	7671
022	2460	3215	2976	3810	2976	3961
μ_{Mn} (μ_B)	2.18(16) //*b*		2.09(15) //*b*		2.24(15) //*b*	
					$\mu_{Ce} = -0.23(12)\mu_B$ //*B*	
R_w	3.2%		3.7%		3.1%	

[a] Assuming ordering of the Ce sublattice.

Pr sublattice, they are quite similar to those observed for $LaMnSi_2$, yielding the same ferromagnetic ordering onto the Mn sublattice (fig. 3). The refined parameters (y and μ_{Mn}) at 300 and 200 K are collected in table 5, as well as the observed and calculated intensities.

At 2 K, additional lines appear in the neutron diffraction pattern, characteristic of an antiferromagnetic ordering, in agreement with the magnetic measurements [5]. Several superlattice lines are observed and the remaining lines are characteristic of the only nuclear scattering with no magnetic contributions (see before). The Bragg angles of the superlattice lines can all be indexed on the basis of the crystal unit cell. They obey the rule $h + k = 2n + 1$ (forbidden by the nuclear translation C) and the $(0k0)$ series are absent. This suggests a simple antiferromagnetic structure based on the magnetic antitranslation C′ for both the Mn and Pr sublattices, the moment direction being along the *b*-axis. In the $TbFeSi_2$ type structure, for each kind of atom, there are four equivalent positions per unit cell which can be separated into two sets of positions not related by the C-translation.

These are, for Pr and Mn:

Pr	0	0.104	$\frac{1}{4}$	AF
	$\frac{1}{2}$	0.604	$\frac{1}{4}$	
	0	0.896	$\frac{3}{4}$	AF
	$\frac{1}{2}$	0.396	$\frac{3}{4}$	
Mn	0	~ 0.750	$\frac{1}{4}$	AF
	$\frac{1}{2}$	~ 0.250	$\frac{1}{4}$	
	0	~ 0.250	$\frac{3}{4}$	AF
	$\frac{1}{2}$	~ 0.750	$\frac{3}{4}$	

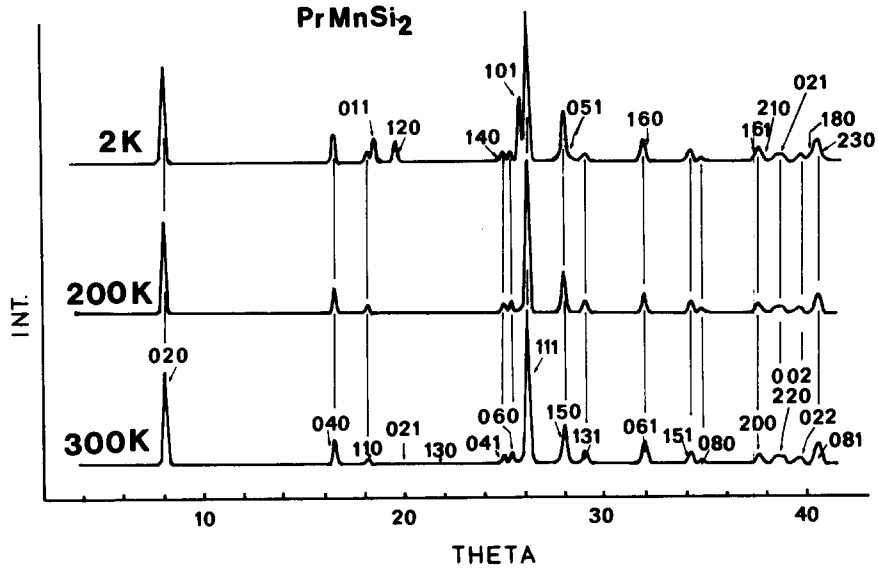

Fig. 4. Neutron diffraction patterns of $PrMnSi_2$ at 300, 200 and 2 K.

with an antiferromagnetic coupling in each set of positions.

All these observations imply that the magnetic structure consists of ferromagnetic (010) planes of Pr atoms with two possible coupling sequences along the *b*-axis: $++--$ or $+---$ while the Mn-sublattice consists of ferro(+) or antiferromagnetic(+/−) (010) planes, antiferromagnetically coupled along the *b*-axis. Furthermore, several kinds of coupling are possible between Mn and Pr layers.

The results of various refinements lead us to retain unambiguously (R = 3.2%), the following scheme: $+(-)+-(+)-$, according to the stacking sequence previously defined as Pr–(Mn)–Pr–Pr–(Mn)–Pr... (fig. 1). Table 6 gives the calculated and observed intensities and also the adjustable parameters (y, μ_{Mn} and μ_{Pr}).

Therefore, below T_N, the magnetic structure of $PrMnSi_2$ consists of ferromagnetic (010) layers of Pr and Mn with moments perpendicular to the layers. Each Mn layer is antiferromagnetically coupled to the two adjacent ferromagnetically coupled Pr layers. This magnetic structure is shown in fig. 5.

Thus, it may be noted that the rare-earth sublattice ordering involves a different magnetic coupling of the Mn sublattice which shifts from ferromagnetic (above T_N) to antiferromagnetic (below T_N).

At 2 K, the Mn-atom magnetic moment is found to be $\mu_{Mn} = 2.35(10)\mu_B$, in agreement with the value observed at higher temperature. For the

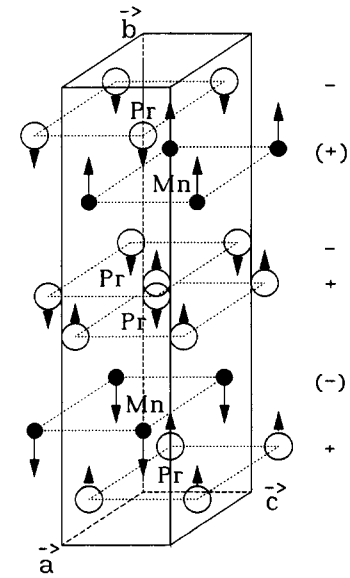

Fig. 5. Magnetic structure of $PrMnSi_2$ at 2 K.

Pr atom, we obtain $\mu_{Pr} = 2.04(4)\mu_B$, a value which is much smaller than that expected for the Pr^{3+} free ion ($3.2\mu_B$). These values imply a total resulting moment of $4.39\mu_B$ per formula unit, in good agreement with those obtained by magnetization measurements (table 1, [5]). The thermal dependence of the magnetic intensities recorded step-by-step between 300 and 2 K gives a Pr-sublattice ordering temperature $T_N = (34 \pm 2)$ K, in fair agreement with the magnetic measurement determinations [5].

4.4. $NdMnSi_2$

The temperature dependence of the neutron diffraction patterns recorded step-by-step from room temperature to 2 K shows the following.

Table 5
$PrMnSi_2$. Calculated and observed intensities, y atomic positions, magnetic moments and reliability factors at 300 and 200 K

hkl	300 K		200 K	
	y_{Pr} = 0.1026(12)	y_{Si1} = 0.3267(11)	y_{Pr} = 0.1023(6)	y_{Si1} = 0.3252(5)
	y_{Mn} = 0.7488(16)	y_{Si2} = 0.4658(18)	y_{Mn} = 0.7500(8)	y_{Si2} = 0.4662(9)
	I_0	I_c	I_0	I_c
020	1.65	1.65	1.75	1.75
040	1.50	1.56	1.53	1.58
110	0.54	0.48	0.53	0.51
021	~ 0.00	0.08	~ 0.00	0.06
130	~ 0.00	0.06	~ 0.00	0.05
041	0.67	0.83	0.75	0.89
060	0.99	1.27	1.30	1.36
111	22.65	21.71	24.18	23.81
150	6.25	6.53	7.35	7.56
131	2.22	2.63	2.85	3.01
061	4.80	5.26	5.67	5.70
151	3.25	3.51	3.82	4.15
080	1.09	1.25	1.64	1.43
200	3.04	3.59	4.27	3.93
002 / 220	5.57	7.46	8.51	8.16
022	2.70	3.87	4.03	4.23
081	8.63	8.95	10.30	9.66
μ_{Mn} (μ_B)	1.93(19) //b		2.06(8) //b	
R_w	4.4%		2.4%	

Table 6
$PrMnSi_2$. Calculated and observed intensities, y atomic positions, magnetic moments and reliability factors at 2 K

hkl	2 K	
	y_{Pr} = 0.0998(7)	y_{Si1} = 0.3223(6)
	y_{Mn} = 0.7551(10)	y_{Si2} = 0.4609(8)
	I_0	I_c
020	1.74	1.75
040	1.56	1.61
110	0.54	0.52
011	1.68	1.71
021	~ 0.00	0.06
120	1.64	1.60
130	~ 0.00	0.00
140	0.52	0.65
041	0.73	0.65
060	0.99	0.83
101	9.00	8.82
111	22.69	22.02
051 / 150	8.00	8.96
131	1.02	1.04
160 / 061	5.48	5.66
151	4.21	4.37
080	2.40	2.54
210 / 161 / 200	8.00	8.73
021 / 002 / 220	7.20	7.08
022	3.50	3.43
180 / 230 / 081	16.00	15.83
μ_{Mn} (μ_B)	2.35(10) //b	
μ_{Pr} (μ_B)	2.04(4) //b	
R_w	3.2%	

(i) between 300 and $T_C' \sim 40$ K: a continuous increase of the intensities of the only nuclear reflections which obey the rule h, k, l of the same parity,

(ii) below 40 K: a increase of the intensities of all the nuclear reflections.

This implies a ferromagnetic ordering for both Mn and Nd (below 40 K) sublattices when decreasing in temperature, in agreement with the magnetometric measurements [5].

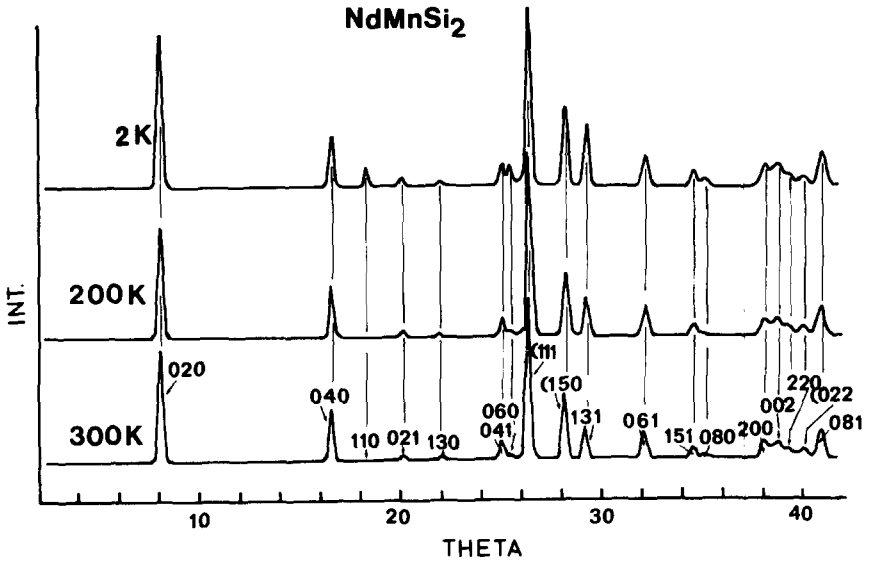

Fig. 6. Neutron diffraction patterns of $NdMnSi_2$ at 300, 200 and 2 K.

Table 7
$NdMnSi_2$. Calculated and observed intensities, y atomic positions, magnetic moments and reliability factors at 300, 200 and 2 K

hkl	300 K		200 K		2 K	
	y_{Nd} = 0.1020(5)	y_{Si1} = 0.3256(6)	y_{Nd} = 0.1019(6)	y_{Si1} = 0.3255(8)	y_{Nd} = 0.1005(7)	y_{Si1} = 0.3266(9)
	y_{Mn} = 0.7533(9)	y_{Si2} = 0.4625(12)	y_{Mn} = 0.7529(14)	y_{Si2} = 0.4652(14)	y_{Mn} = 0.7508(21)	y_{Si2} = 0.4645(13)
	I_0	I_c	I_0	I_c	I_0	I_c
020	8.57	8.70	8.50	8.77	10.36	10.69
040	13.27	13.77	12.76	12.87	12.67	13.00
110	~ 0.00	0.01	~ 0.00	0.01	4.65	4.96
021	1.66	1.73	1.89	1.87	3.23	3.29
130	0.66	0.73	0.86	0.88	1.44	1.57
041	8.04	6.62	8.26	7.26	9.71	9.75
060	1.07	1.44	1.02	1.53	10.92	9.95
111	125.15	124.54	128.03	127.06	119.83	119.23
150	52.23	52.13	52.68	53.82	58.33	58.18
131	28.86	28.90	30.96	30.96	49.31	47.37
061	31.56	31.87	31.05	31.16	32.92	32.62
151	14.98	15.77	15.50	17.15	17.59	18.87
080	5.43	4.40	5.43	3.54	8.98	7.63
081	64.99	65.82	66.50	65.65	72.14	70.89
μ_{Mn} (μ_B)	2.06(15) *//b*		2.48(15) *//b*		2.29(20) in the (011) plane	μ_y = 1.62(15) μ_z = 1.62(25)
μ_{Nd} (μ_B)	–		–		1.80(7) *//c*	
R_w	1.6%		2.1%		2.6%	

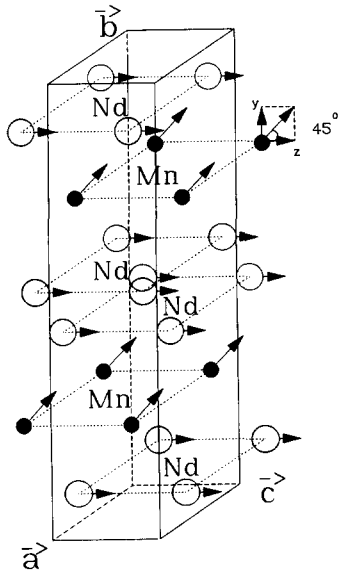

Fig. 7. Magnetic structure of $NdMnSi_2$ at 2 K.

Three neutron diffraction patterns recorded at 300, 200 and 2 K are shown in fig. 6.

At 300 and 200 K, they are quite similar to those observed for $LaMnSi_2$ and $PrMnSi_2$, yielding the same ferromagnetic ordering as that of the Mn-sublattice (fig. 3). The refined parameters (y and μ_{Mn}) are collected in table 7 along with the observed and calculated intensities.

At 2 K, both Mn and Nd sublattices are ferromagnetic and the occurrence of the ($0k0$) reflections (by contrast to high temperatures patterns) may be due to the rise of a magnetic component perpendicular to the b-axis, either on Nd or Mn sites, or both. The best fits ($R = 2.6\%$) clearly show that both Nd and Mn magnetic moments lie in the (011) plane, along [001] and at 45° of this direction for Nd and Mn, respectively. Table 7 gives the calculated and observed intensities as also the adjustable parameters (y, μ_{Mn} and μ_{Nd}).

Thus, the Nd-sublattice ordering goes with a spin reorientation of the Mn-sublattice. The magnetic structure is shown in fig. 7. Here again, it consists of ferromagnetic (010) planes of R and Mn atoms, respectively, stacked along the b-axis.

The value of the magnetic moment of the Mn atoms ($\mu_{Mn} = 2.3(2)\mu_B$) is in agreement with that observed at higher temperatures. As in $PrMnSi_2$, the Nd magnetic moment ($\mu_{Nd} = 1.80(7)\mu_B$) is strongly reduced with respect to the free ion value ($3.27\mu_B$). The total resulting moment ($\approx 4.10\mu_B$ per formula unit) and the T_C' value determined from thermal dependence of the magnetic intensities ($T_C' = (40 \pm 3)$K) are in good agreement with the magnetic measurement determinations (table 1, [5]).

5. Discussion

In this paper, a neutron diffraction study of the magnetic properties of the $RMnSi_2$ (R = La, Ce, Pr, Nd) series is reported. In the introduction, we have emphasized the straight relationships between the $ThCr_2Si_2$, α $ThSi_2$ and $TbFeSi_2$ type structure, i.e. the $TbFeSi_2$ type structure could be described as isolated $ThCr_2Si_2$ type blocks (containing the Mn planes) connected via α $ThSi_2$ slabs. Here, as in the corresponding RMn_2X_2(X = Si, Ge) compounds, we observed magnetic ordering of the Mn-sublattices.

It is of interest at first to compare the Mn magnetic behaviour in the new silicides $RMnSi_2$ and in the silicides or germanides isotypic with $ThCr_2Si_2$: RMn_2 (Si, Ge)$_2$ (table 8). Large analogies appear, some are predictable, but others are surprising when taking into account the parentage but also some peculiarities of the two structure types $TbFeSi_2$ and $ThCr_2Si_2$. In the pseudo-lamellar structures of these different ternary compounds, there are the same Mn atoms planes with a tetrahedral coordination of the non-metal atoms: (010) planes in the $TbFeSi_2$, and (001) in the $ThCr_2Si_2$ isotypic compounds. The distances between nearest neighbours atoms are short: 2.97 Å $> d^1_{Mn-Mn} >$ 2.74 Å (fig. 8). In these planes, it seems "normal" that the magnetic interactions remain nearly of the same magnitude: they always are ferromagnetic and probably strong, in agreement with the Slater–Néel curve, and the experimental Curie temperatures (table 1).

According to the neutron investigation, the Mn magnetic moment values (tables 3–7) in the $RMnSi_2$ compounds (R = La, Ce, Pr, Nd) are close to those measured in the RMn_2X_2 (X = Si, Ge) silicides and germanides, isotype of $ThCr_2Si_2$.

In these last compounds, μ_{Mn} consists of between 1.5 and 2.5μ_B [4,9–11]. This analogy seems reasonable since Mn has the same coordination in the two parent structures. Moreover, it may be noted that the values are close to those observed in various binary and ternary intermetallic compounds [12].

Despite of the structure and composition changes between the two phases, the ordering temperatures T_{Mn} of the Mn sublattices are very high and close to each other. For each of the homogeneous groups $RMnSi_2$, RMn_2Si_2 and RMn_2Ge_2, between 300 and 470 K, T_{Mn} slowly increases as compared with the rare-earth contraction.

Whereas it seems obvious to find nearly the same interactions within the Mn planes, it is surprising that the interactions between successive planes are not very different in the $ThCr_2Si_2$ isotype and $TbFeSi_2$ isotype series. Even in the $ThCr_2Si_2$ isotype compounds, these planes are rather far from each other, ($d^2_{Mn-Mn} > 5.2$ Å, fig. 8). Their interactions should be weaker than those acting within the planes. Superexchange couplings via Si or Ge atoms have been proposed but not really confirmed [4].

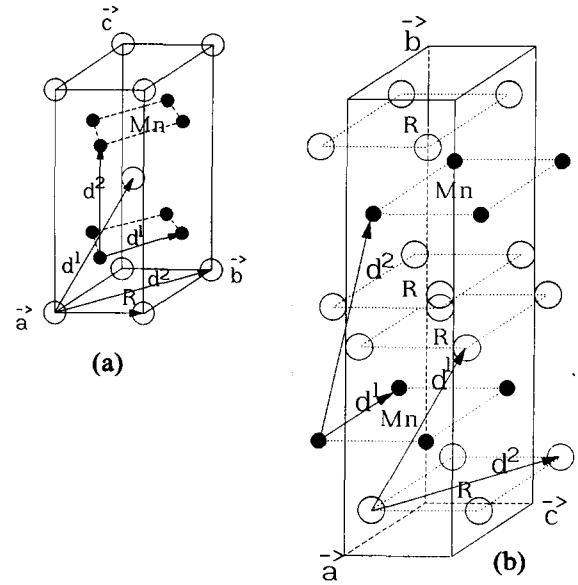

Fig. 8. Mn–Mn and R–R interatomic distances in (a) $ThCr_2Si_2$ and (b) $TbFeSi_2$ type structures.

Table 8
$RMnSi_2$ and $RMn_2(Si, Ge)_2$ compounds. Interatomic distances and magnetic couplings in the Mn sublattice [4,5] [a]

Compounds	Distances (Å)		Magnetic couplings		$T_{C,N}$ (K)
	d_1 (Mn–Mn)	d_2 (Mn–Mn)			
	intra-layer	inter-layer	intra-layer	inter-layer	
$LaMnSi_2$	2.92	8.89	F	F	386
$CeMnSi_2$	2.88	8.83	F	F	398
$PrMnSi_2$	2.87	8.82	F	F	434
$NdMnSi_2$	2.86	8.79	F	F	441
$SmMnSi_2$	2.84	8.75	F	F	464
$LaMn_2Ge_2$	2.97	5.49	F	F	306
$CeMn_2Ge_2$	2.92	5.46	F	F	322
$PrMn_2Ge_2$	2.91	5.45	F	F	334
$NdMn_2Ge_2$	2.90	5.45	F	F	334
$SmMn_2Ge_2$	2.88	5.42	F	F	348
				AF	196
$GdMn_2Ge_2$	2.85	5.45	F	AF	365
$LuMn_2Ge_2$	2.78	5.40	F	AF	453
$LaMn_2Si_2$	2.91	5.30	F	F	303
$CeMn_2Si_2$ [b]	2.85	5.28	F	AF	379
$PrMn_2Si_2$	2.85	5.28	F	AF	348
$NdMn_2Si_2$	2.83	5.27	F	AF	365
$SmMn_2Si_2$	2.81	5.25	F	AF	398
$LuMn_2Si_2$	2.74	5.20	F	AF	464

[a] F: ferromagnetic; AF: antiferromagnetic; $T_{C,N}$: Curie or Néel temperatures.
[b] Ce tetravalent.

In the $TbFeSi_2$ isotype compounds, the interplanar distance (fig. 8) is close to 9 Å and the interactions cannot be other type than RKKY, via the conduction electrons.

In the $RMn_2(Si, Ge)_2$ compounds, the couplings between Mn layers are observed to be either ferro- or antiferromagnetic (table 8). The sign of the Mn–Mn interlayer exchange coupling constant appears to be sensitive to the lattice spacing, i.e. to the Mn–Mn separation. To the magnetic ordering temperature of the RMn_2X_2 compounds, expressed in terms of the most significant Mn–Mn distances (see fig. 4 in ref. [13] and fig. 4 in ref. [14]), corresponds an universal curve when plotted versus d^1_{Mn-Mn} (intralayer) but not versus d^2_{Mn-Mn} (interlayer). There is a critical distance of $d_{Mn-Mn} \approx 2.850$ Å, where the coupling between the interlayer Mn moments is antiferromagnetic for

$d_{Mn-Mn} < 2.850$ Å and becomes ferromagnetic for $d_{Mn-Mn} \approx 2.850$ Å. A similar critical distance has been observed in many Mn alloys with transition metals [15]. This critical distance is close to the value (≈ 2.85 Å) proposed by Goodenough on the assumption of localized/delocalized 3d electrons [16].

This empiric classification is somewhat surprising; however, the $RMnSi_2$ silicides obey it rather well, although they do not have the same structural type.

Furthermore, it is worth noting that in the new $RMnSi_2$ silicides the magnetic moments are perpendicular to the layers, as observed in the RT_2X_2 ($ThCr_2Si_2$ type structure) compounds, according to the strong anisotropic character of both series of compounds.

On the other hand, it should be noted that the analogy in the magnetic behaviour between $RMnSi_2$ and RMn_2X_2 compounds (R = light rare earths) does not apparently spread to the rare-earth atoms, as no magnetic ordering has been observed on the rare-earth sublattice in the later series (expected in $SmMn_2Ge_2$ [17] and perhaps $NdMn_2Si_2$ [4,18]). Moreover, Ce is trivalent in $CeMnSi_2$ (5), whereas a recent study has shown that it has an intermediate valence state in $CeMn_2Si_2$ [19].

The second remark concerns the low-temperature magnetic structures of the $RMnSi_2$ (R = La–Sm) series. First, we can remark that Pr and Nd order at a relatively high temperature (~ 40 K), whereas Sm does not seem to present any ordering down to 2 K. In the case of $CeMnSi_2$, the situation is more complicated and further investigations at very low temperature (< 1.3 K) are in progress.

Once again, the $RMnSi_2$ (R = Pr, Nd) series appears anomalous when considering the R–Mn couplings on one hand and the easy axis direction on the other one.

From the neutron diffraction studies, the result is that the R magnetic moments lie in the basal plane ($0k0$) in $NdMnSi_2$, contrary to the $PrMnSi_2$ case. It should be noted that Takano has already calculated for Nd magnetic moment a possible deviation from the main axis of the $ThCr_2Si_2$ type structure of $\Phi = 36°$ [19]. More recently, such an orientation for Nd magnetic moment was observed in the α $ThSi_2$ structure [20], the R–Si stacking sequence of which is also that observed in the $NdMnSi_2$ structure (see introduction). Such a difference in the Pr and Nd magnetic moment directions has been already encountered in $ThCr_2Si_2$ type structure compounds, for example, in the RNi_2Si_2 and RCu_2Si_2 series [22,23].

The nature of the transition metal also seems to be important. In the isotype series $RFeSi_2$ [24] the moments align along the b-axis in both $PrFeSi_2$ and $NdFeSi_2$.

The next remark relates to the R–Mn couplings. In the case of $NdMnSi_2$, the R magnetic ordering yields a spin-reorientation phenomena. Iwata et al. [10] have shown that, for light rare earths, the ferromagnetic coupling between the rare earth and Mn sublattices is dominant. Therefore, this interaction and the in-plane orientation of the Nd moment allow one to stabilize a canted magnetic structure down to 40 K. However, the reorientation of the Mn moment is only partial and gives evidence of the strong anisotropy of the easy axis magnetization axis of Nd and Mn from which the observed behaviour probably originates.

For $PrMnSi_2$ (and probably in $CeMnSi_2$), the situation appears more complicated in terms of exchange couplings since the R–Mn interactions are negative at short distances (nearest neighbours, $d = 3.23$ and 3.25 Å) and positive for the next nearest neighbours ($d = 6.20$ and 6.83 Å) (fig. 5).

It is of interest to remark that the situation is fully reversed in the $RFeSi_2$ series. Thus, $PrFeSi_2$ is ferromagnetic, whereas $NdFeSi_2$ is antiferromagnetic. However, in these compounds, Fe has no magnetic moment. The rare-earth sublattice ordering temperature is 6 and 26 K for $NdFeSi_2$ and $PrFeSi_2$, respectively [5,24], whereas it is close to 40 K for both $NdMnSi_2$ and $PrMnSi_2$. This difference of 15 to 35 K reflects the strength of the R–T exchange interactions, for a part depending on the nature of the transition metal T.

The last remark concerns the magnitude of the rare-earth magnetic moments observed in $RMnSi_2$ compounds. The values deduced from the neutron diffraction experiments are considerably reduced in comparison with the theoretical ones (i.e. $\sim 1.9\mu_B$ instead of $3.2\mu_B$ for the R^{3+} free ions,

tables 6 and 7). The formal charge attributed to the 3d metal has probably a large effect on the crystal field scheme since the 3d metal environment of the R-site is very asymmetric (fig. 1). Here again, the nature of the transition metal appears to be important since smaller reductions are observed in the corresponding $RFeSi_2$ compounds (e.g., $\sim 2.5\mu_B$ [24]). Such reductions are not observed in RMn_2X_2 parent compounds where the R local symmetry is much higher.

6. Conclusion

The analysis of the magnetic ordering of $RMnSi_2$ (R = La, Ce, Pr, Nd) compounds provides interesting information about the magnetic anisotropy and exchange interactions in this series.

The localized moments, both on 4f and 3d atoms, interact directly and indirectly via the itinerant electrons. The direction and magnitude of the ordered R magnetic moments depend on the local crystal electric field (CEF).

At high temperature, ferromagnetic ordering of the Mn sublattice was found in all the compounds presently investigated, with a Mn magnetic moment of about 2 to $2.5\mu_B$ aligned along the stacking axis of the structure. Comparison with the parent RMn_2X_2, $ThCr_2Si_2$ type structure compounds, shows that the sign of the Mn–Mn interlayer exchange parameter seems to be sensitive to the Mn–Mn intralayer separation. In this scheme, $SmMnSi_2$ appears to be a very interesting case. One can notice that, at room temperature, the d(Mn–Mn) distance in this compound is close to the limit value (≈ 2.85 Å) which separates antiferromagnetic to ferromagnetic behaviour. In order to find this point precisely, magnetometric measurements under external pressure are underway on $SmMnSi_2$.

As regards the interlayer interactions, a theoretical analysis would be needed; firstly, in the case of the $ThCr_2Si_2$ isotype compounds ($d_{Mn-Mn} \sim 5$ Å), and seemly with more reason in the $TbFeSi_2$ isotype series, where the 2-D character of the Mn-sublattice is still more marked ($d_{Mn-Mn} = 9$ Å).

The various low-temperature magnetic structures found in $PrMnSi_2$ and $NdMnSi_2$ compounds belong to several magnetic configurations. The magnetic properties mostly depend on two main terms: the exchange interactions described by the RKKY model and the crystal electric field strength. Comparisons of $RMnSi_2$, $RFeSi_2$ and RT_2X_2 series permit to point out that, at low temperature, the exchange interactions between R and Mn atoms act significantly on the magnetism. Furthermore, the magnetic configurations depend not only on the R-ion but also vary with the transition metal element T. At low temperature, the direction of the magnetic moment is not fixed for a given T, but the easy direction is determined by crystal electric field acting on the R-ions. Orientation of the magnetic moment is connected with the sign of the B_2^0 CEF coefficient which is in turn determined by the Stevens second-order parameters, the α_j and A_2^0. According to Greedan and Rao [25], a positive value of B_2^0 indicates that R magnetic moments lie in the basal plane, or deviate significantly from the main axis. As the sign of A_2^0 remains constant for a given site, in $NdMnSi_2$ and $PrMnSi_2$, the easy axis is probably correlated to the sign of α_j.

In another way, determination of the a/c ratio for a large number of RT_2X_2 compounds allows one to remark that an oscillatory magnetic ordering is stabilized for $a/c > 0.408$, i.e. $d^2_{R-R} > d^1_{R-R}$ (fig. 8) [26–28]. This criterion seems to run again for the $RTSi_2$ series, as it could be observed for $PrFeSi_2$ and $NdFeSi_2$ [24]. For the $RMnSi_2$ compounds, the criterion is never satisfied and the related magnetic structure of $PrMnSi_2$ and $NdMnSi_2$ are commensurate with the crystal lattice.

The magnitude of the R magnetic moments in $RMnSi_2$ and $RFeSi_2$ are somewhat smaller (depending on T) than the corresponding free-ion values, contrarily to the RT_2X_2 compounds. Most likely, this must be attributed to CEF effects. The interesting panel of magnetic configurations setting on R and on the T sublattices is perhaps sustained by the conduction electron density which is mainly due to the T element. In order to gain more precision on this point, further investigations on quaternary R(Mn, Fe)Si_2 compounds are in progress.

Acknowledgements

Neutron diffraction data were recorded at the Institut Laue Langevin (ILL). We are grateful to J.L. Soubeyroux, responsible for the spectrometer used, for his help during the measurements.

References

[1] V.I. Yarovets and Yu.K. Gorelenko, Vestn. L'vovsk Univ. Ser. Khim. 23 (1981) 20.
[2] O.I. Bodak and E.I. Gladyshevskii, Sov. Phys. Crystallogr. 14 (1970) 859.
[3] G. Brauer and A. Mitius, Z. Anorg. Allg. Chem. 249 (1942) 325.
[4] J. Leciejewicz and A. Szytuła, in: Handbook on the Physics and Chemistry of Rare Earths, vol. 12, eds. K.A. Gschneidner, Jr. and L. Eyring (North-Holland, Amsterdam, 1989) p. 133.
[5] G. Venturini, B. Malaman, M. Meot-Meyer, D. Fruchart, G. le Caer, D. Malterre and B. Roques, Rev. Chim. Min. 23 (1986) 162.
[6] A.J. Freeman and J.P. Desclaux, J. Magn. Magn. Mat. 12 (1979) 11.
[7] C. Stassis, H.W. Deckmann, B.N. Harmon, J.P. Desclaux and A.J. Freeman, Phys. Rev. B 15 (1977) 369.
[8] P. Wolfers, System MXD, Library of Programs, Laboratoire de Cristallographie, Grenoble, France.
[9] T. Shigeoka, N. Iwata, H. Fujii and T.J. Okamoto, J. Magn. Magn. Mat. 53 (1985) 83.
[10] N. Iwata, T. Ikeda, T. Shigeoka, H. Fujii and T.J. Okamoto, J. Magn. Magn. Mat. 54–57 (1985) 481.
[11] T. Shigeoka, J. Sci. (Hiroshima University) 48 (1984) 103.
[12] A. Oleś, S. Kajzar, M. Kucab and W. Sikora, Polska Acad. Nauk, Commited Physiki, Warsaw (Cracow, 1976).
[13] H. Fujii, T.J. Okamoto, T. Shigeoka and N. Iwata, Solid State Commun. 53 (1986) 715.
[14] A. Szytuła and S. Siek, J. Magn. Magn. Mat. 27 (1982) 49.
[15] R.S. Tebble and D.J. Craik, Magnetic Materials (John Wiley, New York, 1969) p. 61.
[16] J.B. Goodenough, Magnetism and Chemical Bond (John Wiley, New York, 1963) p. 240.
[17] M. Duraj, R. Duraj, A. Szytuła and Z. Tomkowicz, J. Magn. Magn. Mat. 73 (1988) 240.
[18] B. Chofik, I. el Idrissi et al., submitted to Solid State Commun.
[19] G. Liang, I. Perez, D. Dimarzio, M. Craft, D.C. Johnston, N. Anbalagon and T. Mihalisin, Phys. Rev. B 37 (1988) 5970.
[20] Y. Takano, K. Ohhata and K. Sekisawa, J. Magn. Magn. Mat. 70 (1987) 242.
[21] J. Pierre, B. Lambert-Andron and J.L. Soubeyroux, J. Magn. Magn. Mat. 81 (1989) 39.
[22] J.M. Barandanian, D. Gignoux, D. Schmitt, J.C. Gomez-Sal and J. Rodriguez, J. Magn. Magn. Mat. 69 (1987) 61.
[23] J. Leciejewicz, M. Kolendo and A. Szytuła, J. Magn. Magn. Mat. 53 (1986) 309.
[24] B. Malaman, G. Venturini, G. le Caër, L. Pontonnier, D. Fruchart, K. Tomala and J.P. Sanchez, Phys. Rev. B 41 (1990) 4700.
[25] J.E. Greedan and Rao, J. Solid State Chem. 6 (1973) 387.
[26] M. Francois, PhD. Thesis, Nancy, France (1986).
[27] C. Godart, L.C. Gupta and M.F. Ravet-Krill, J. Less Comm. Met. 94 (1983) 187.
[28] J. Leciejewicz and A. Szytuła, J. Magn. Magn. Mat. 63&64 (1987) 190.